Interaction and Multiscale Mechanics, *Vol. 6, No. 2 (2013) 107-125*
DOI: http://dx.doi.org/10.12989/imm.2013.6.2.107

Meshfree consolidation analysis of saturated porous media with stabilized conforming nodal integration formulation

Dongdong Wang*[1], Pinkang Xie[1] and Hongsheng Lu[2]

[1]*Department of Civil Engineering, Xiamen University, Xiamen, Fujian 361005, China*
[2]*Shanghai Hengstar Technology Co. Ltd., Shanghai 201203, China*

(Received March 5, 2013, Revised May 1, 2013, Accepted May 5, 2013)

Abstract. A strain smoothing meshfree formulation with stabilized conforming nodal integration is presented for modeling the consolidation process in saturated porous media. In the present method, nodal strain smoothing is consistently introduced into the meshfree approximation of strain and pore pressure gradient variables associated with the saturated porous media. Meanwhile, in order to achieve a consistent numerical implementation, a smoothing approximation of the meshfree shape function within a nodal representative domain is also proposed in the stiffness construction. The resulting discrete system of equations is all expressed in smoothed nodal measures that are very efficient for numerical evaluation. Subsequently the space-time fully discrete equations are further established by the generalized trapezoidal rule for time integration. The effectiveness of the proposed meshfree consolidation analysis method is systematically illustrated by several benchmark problems.

Keywords: meshfree method; consolidation; saturated porous media; strain smoothing; stabilized conforming nodal integration

1. Introduction

During the past two decades meshfree methods have experienced substantially fast developments and up to date they have evolved into a very important class of numerical methods which are very attractive for various scientific and engineering problems often posing severe difficulties for the conventional finite element method, i.e., high order problems, large deformation and moving boundary problems, etc (Atluri and Shen 2002, Babuška *et al.* 2003, Li and Liu 2004, Liu 2009). However, computational efficiency has been one major concern for the meshfree methods, especially the popular Galerkinmeshfree methods such as element free Galerkin method (Belytschko *et al*. 1994) and reproducing kernel particle method (Liu *et al*. 1995, Chen *et al*. 1996) in which the moving least square (Lancaster and Salkauskas 1981) or reproducing kernel shape functions (Liu *et al*. 1995) are used. One important reason that lowers the computational efficiency is that due to the non-polynomial property of the meshfree shape function, high order Gauss quadrature rule is commonly needed to ensure the integration accuracy of the weak form. To circumvent this deficiency of Galerkinmeshfree methods, nodal integration with least square

*Corresponding author, Professor, E-mail: ddwang@xmu.edu.cn

http://www.techno-press.org/?journal=imm&subpage=7 ISSN: 1976-0426 (Print), 2092-6200 (Online)

residual stabilization was proposed by Beissel and Belytschko (1996). Chen *et al.* (2001, 2002) proposed the integration constraints of Galerkin meshfree methods and developed the stabilized conforming nodal integration (SCNI) method. SCNI systematically brings in the strain smoothing methodology (Chen *et al*. 2000, 2001) for stability and simultaneously inherits the efficient merit of nodal integration without artificial parameters. Subsequently this method was further developed and generalized for plate and shell problems (Wang and Chen 2004, 2008, Chen and Wang 2006, Wang and Lin 2011), geomechanics problems (Wang *et al*. 2011) and fragment-impact problems (Guan *et al*. 2011). More details about the recent development of stabilized Galerkin meshfree methods can be found in the review paper by Chen *et al*. (2011).

In this work we aim to develop an efficient Galerkin meshfree method for consolidation analysis within the stabilized conforming nodal integration framework. The consolidation in porous media is an important problem in foundation engineering, in which the solid skeleton displacement and pore pressure are sought simultaneously. The consolidation modeling considered herein is based upon the generalized Biot consolidation formulation (Biot 1941, 1956, Zienkiewicz and Shiomi 1984). The numerical simulation analysis of consolidation problems have been discussed extensively in the category of finite element methods, e.g., Zienkiewicz and Shiomi (1984), Cui *et al*. (1996), Korsawe *et al*. (2006) and the references therein. In the meshfree context, recently a smoothed radial point interpolation method and the element free Galerkin method were proposed for consolidation simulations (Schönewald *et al*. 2012, Samimi and Pak 2012). In the present study we consistently introduce the strain smoothing nodal integration Galerkin MLS/RK meshfree formulation into the consolidation analysis of saturated porous media. Firstly both the strain and the gradient of pore pressure are expressed in nodal smoothing forms with the smoothed meshfree shape function gradient defined as a boundary integral of the nodal representative domain. Thereafter to keep a consistent computational format with the gradient evaluation, a smoothed nodal shape function in the nodal representative domain is also defined as an average of the boundary contour integral of the shape function. Meanwhile the proposed smoothed nodal shape function is used for the computation of external forces in a unified nodal integration approach. We find this formulation is very convenient from the computational point of view which gives excellent numerical performance.

The paper is organized as follows. Section 2 briefly summarizes the fundamentals of consolidation theory including the momentum balance and continuity equations. The meshfree approximation, strain smoothing formulation and nodally integrated discrete meshfree equations are presented in Section 3. In Section 4 several benchmark problems are tested to demonstrate the proposed meshfree algorithm. Finally concluding remarks are given Section 5.

2. Preliminaries of consolidation theory

2.1 Momentum balance equation

A fully saturated porous media is a two-phase continuum that consists of the solid phase and the fluid phase. According to the well-known Biot's consolidation theory (Biot 1941, 1956, ienkiewicz and Shiomi984), the primary variables for the dynamic behavior of a fully saturated porous media are the solid skeleton displacement u and the fluid pore pressure p. With the common assumption of ignoring the inertia effect, the momentum balance equation for the total system with solid and fluid can be stated as

$$\sigma_{ij,j} + \rho b_i = 0 \tag{1}$$

where σ_{ij} is the total stress in the solid and fluid mixture, b_i is the body force and ρ is the density of the mixture, respectively.

Moreover, for the solid skeleton, the so-called effective stress $\sigma_{ij}^{"}$ can be defined as

$$\sigma_{ij}^{"} = \sigma_{ij} + \alpha\delta_{ij} p \tag{2}$$

where σ_{ij} is the total stress, δ_{ij} is the Kronecker delta, α is the Biot-Willis coefficient to describe the compressibility of the solid phase. Assume the solid undergoes linear elastic deformation, the effective stress $\sigma_{ij}^{"}$ is related to the strain ε_{kl} as

$$\sigma_{ij}^{"} = C_{ijkl}\varepsilon_{kl}, \quad \varepsilon_{kl} = (u_{k,l} + u_{l,k})/2 \tag{3}$$

where C_{ijkl} is the elasticity tensor, in case of isotropic elasticity $C_{ijkl} = K\delta_{ij}\delta_{kl} + \mu(\delta_{ik}\delta_{jl} + \delta_{il}\delta_{jk})$, K and μ are the bulk modulus and the shear modulus of the solid skeleton. Generally the pore pressure *p* only introduces volumetric deformation ε_{ij}^{p}, i.e.

$$\varepsilon_{ij}^{p} = -\delta_{ij}\frac{1}{3K_s} p \tag{4}$$

in which K_s is the bulk modulus of the solid grain.

On the other hand, the total stress σ_{ij} in the porous media can also be split into two parts as

$$\sigma_{ij} = \sigma_{ij}^{'} - \delta_{ij} p \tag{5}$$

where $\sigma_{ij}^{'}$ is known as the true effective stress that is contributed by the deformation beyond the volumetric deformation ε_{ij}^{p}

$$\sigma_{ij}^{'} = C_{ijkl}(\varepsilon_{kl} - \varepsilon_{kl}^{p}) \tag{6}$$

A direct comparison of Eqs. (2) and (5) implies the relationship between the effective stress $\sigma_{ij}^{"}$ and the true effective stress $\sigma_{ij}^{'}$

$$\sigma_{ij}^{"} = \sigma_{ij}^{'} - (1-\alpha)\delta_{ij} p \tag{7}$$

Further plugging Eqs. (3) and (6) into Eq. (7) gives

$$C_{ijkk}\frac{1}{3K_s} p - (1-\alpha)\delta_{ij} p = 0 \tag{8}$$

where use is made of Eq. (4). Consequently with Eq. (8) the Biot-Willis coefficient α is given by

$$\alpha = 1 - \frac{\delta_{ij} C_{jilk} \delta_{kl}}{9K_s} = \frac{K_s - K}{K_s} \tag{9}$$

Therefore α measures the relative difference between the solid grain bulk modulus and that of the solid skeleton. Finally with α in hand, by using Eq. (2), the equation of motion of Eq. (1) becomes

$$\sigma''_{ij,j} - \alpha p_{,i} + \rho b_i = 0 \tag{10}$$

2.2 Continuity equation

The continuity equation for the fluid phase represents the mass conservation that can be derived through the rate of change of fluid within a unit volume

$$\underbrace{\dot{\varepsilon}_{ii} + \frac{\dot{p}}{K_f} + (1 - \ddot{y})\frac{\dot{p}}{K_s} - \frac{1}{3}\delta_{ij}\frac{\dot{\sigma}'_{ij}}{K_s}}_{\text{Rate of volume increase}} = -\underbrace{q_{i,i}}_{\text{Rate of flow out of volume}} \tag{11}$$

where $\ddot{y}$ is the porosity of the porous media, K_f is the bulk modulus of the fluid. $\dot{\varepsilon}_{ii}$ denotes the volumetric strain rate of the skeleton without volumetric change of grains, $\ddot{y}\dot{p}/K_f$ is the compressive strain rate in fluid, $(1-\ddot{y})\dot{p}/K_s$ is the compressive strain rate in grains due to the pore pressure, $\delta_{ij}\dot{\sigma}'_{ij}/(3K_s)$ represents the change of compression of solid grains due to effective stress change, q_i is the fluid flow rate. With the aid of the relationships of (6) and (9), Eq. (11) reduces to

$$\alpha\dot{\varepsilon}_{ii} + \frac{1}{K_c}\dot{p} + q_{i,i} = 0 \tag{12}$$

where K_c is the combined compressibility parameter given by

$$K_c = \frac{K_s K_f}{K_s + (\alpha - \ddot{y})K_f} \tag{13}$$

Meanwhile, according to the Darcy's law without the inertia effect, the fluid flow rate q_i is defined as

$$q_i = -\kappa(p_{,i} - \rho_f g_i) \tag{14}$$

where ρ_f is the fluid density, g_i is the gravity, κ is the permeability which is related to the intrinsic permeability $\hat{\kappa}$ and the fluid viscosity μ_f as follows

$$\kappa = \frac{\hat{\kappa}}{\mu_f} \tag{15}$$

Eqs. (10) and (12) constitute the set of coupled equations governing the consolidation process of porous medium in a domain Ω with boundary Γ. The corresponding weak forms for these two equations are

$$\begin{cases} \int_\Omega \delta\varepsilon_{ij} C_{ijkl} \varepsilon_{kl} d\Omega - \int_\Omega \delta u_{i,i} \alpha p d\Omega = \int_\Omega \delta u_i \rho b_i d\Omega + \int_{\Gamma^t} \delta u_i \overline{t}_i d\Gamma \\ \int_\Omega \delta p_{,i} \kappa p_{,i} d\Omega + \int_\Omega \delta p \alpha \dot{\varepsilon}_{ii} d\Omega + \int_\Omega \delta p \dot{p} / K_c d\Omega = \int_\Omega \delta p_{,i} \kappa \rho_f g_i d\Omega + \int_{\Gamma^q} \delta p \overline{q}_n d\Gamma \end{cases} \tag{16}$$

where $\overline{t}$ is the applied traction of effective stress on the natural boundary Γ^t, $\overline{q}_n$ is the given fluid flux rate described on the boundary Γ^q.

3. Meshfree strain smoothing formulation

3.1 Meshfree approximation

The meshfree approximation is characterized by constructing the approximant $u^h(\mathbf{x},t)$ of a filed variable $u^h(\mathbf{x},t)$ through a set of *NP* nodes $\{\mathbf{x}_I\}_{I=1}^{NP}$ distributed in the problem domain.

$$u^h(\mathbf{x},t) = \sum_{I=1}^{NP} \Psi_I(\mathbf{x}) d_I(t) \tag{17}$$

where $\Psi_I(\mathbf{x})$ and $d_I(t)$ are the meshfree shape function and nodal coefficient associated with the node $\mathbf{x}_I$. With the employment of moving least square or reproducing kernel approximation theory (Liu *et al*. 1995, Chen *et al*. 1996), $\Psi_I(\mathbf{x})$ takes the following form

$$\Psi_I(\mathbf{x}) = \mathbf{h}^T(\mathbf{x}_I - \mathbf{x})\mathbf{a}(\mathbf{x})\varphi_a(\mathbf{x}_I - \mathbf{x}) \tag{18}$$

in which φ_a is the kernel function with support size "*a*" for controlling the locality and smoothness of the meshfree approximation, in this study it is taken as the classical cubic B-spline function (Chen *et al*. 1996). $\mathbf{h}(\mathbf{x})$ is a vector containing the monomial basis functions up to n-th order

$$\mathbf{h}(\mathbf{x}) = \{1,\ x,\ y,\ x^2,\ xy,\ y^2, ..., x^n,\ ...,\ y^n\}^T \tag{19}$$

and $\mathbf{a}(\mathbf{x})$ is the unknown coefficient vector that is obtained via imposing the following *n*-th order consistence condition

$$\sum_{I=1}^{NP} \Psi_I(\mathbf{x}) x_I^i y_I^j = x^i y^j, \quad 0 \le i+j \le n \tag{20}$$

Substituting Eq. (18) into Eq. (20) gives

$$\mathbf{M}(\mathbf{x})\mathbf{a}(\mathbf{x}) = \mathbf{h}(\mathbf{0}) \tag{21}$$

where $\mathbf{M}(\mathbf{x})$ is the moment matrix

$$\mathbf{M}(\mathbf{x}) = \sum_{I=1}^{NP} \mathbf{h}^T(\mathbf{x}_I - \mathbf{x})\mathbf{h}(\mathbf{x}_I - \mathbf{x})\varphi_a(\mathbf{x}_I - \mathbf{x}) \tag{22}$$

Therefore we have $\mathbf{a}(\mathbf{x}) = \mathbf{M}^{-1}(\mathbf{x})\mathbf{h}(\mathbf{0})$ from Eq. (21) and the meshfree shape function reads

$$\Psi_I(\mathbf{x}) = \mathbf{h}^T(\mathbf{0})\mathbf{M}^{-1}(\mathbf{x})\mathbf{h}(\mathbf{x}_I - \mathbf{x})\varphi_a(\mathbf{x}_I - \mathbf{x}) \tag{23}$$

3.2 Meshfree discretization of consolidation problem

Introducing the meshfree approximation into the displacement *u* and the pore pressure *p* of a porous media under consolidation gives

$$\begin{cases} \mathbf{u}^h(\mathbf{x},t) = \sum_{I=1}^{NP} \Psi_I(\mathbf{x})\mathbf{d}_I(t) \\ \dot{\mathbf{u}}^h(\mathbf{x},t) = \sum_{I=1}^{NP} \Psi_I(\mathbf{x})\dot{\mathbf{d}}_I(t) \\ p^h(\mathbf{x},t) = \sum_{I=1}^{NP} \Psi_I(\mathbf{x}) p_I(t) \\ \dot{p}^h(\mathbf{x},t) = \sum_{I=1}^{NP} \Psi_I(\mathbf{x}) \dot{p}_I(t) \end{cases} \tag{24}$$

Thus the approximate strain vector $\boldsymbol{\varepsilon}^h$ becomes

$$\boldsymbol{\varepsilon}^h(\mathbf{x},t) = \begin{Bmatrix} \varepsilon_{xx}^h \\ \varepsilon_{yy}^h \\ 2\varepsilon_{xy}^h \end{Bmatrix} = \sum_{I=1}^{NP} \mathbf{B}_I^u(\mathbf{x})\mathbf{d}_I(t) \tag{25}$$

with

$$\mathbf{B}_I^u(\mathbf{x}) = \begin{bmatrix} \Psi_{I,x}(\mathbf{x}) & 0 \\ 0 & \Psi_{I,y}(\mathbf{x}) \\ \Psi_{I,y}(\mathbf{x}) & \Psi_{I,x}(\mathbf{x}) \end{bmatrix} \tag{26}$$

Similarly the approximation of the pressure gradient reads

$$\nabla p = \begin{Bmatrix} p_{,x} \\ p_{,y} \end{Bmatrix} = \sum_{I=1}^{NP} \mathbf{B}_I^p(\mathbf{x}) p_I(t) \tag{27}$$

with

$$\mathbf{B}_I^p(\mathbf{x}) = \begin{Bmatrix} \Psi_{I,x}(\mathbf{x}) \\ \Psi_{I,y}(\mathbf{x}) \end{Bmatrix} \tag{28}$$

with the aid of Eqs. (25) and (28), it is straightforward to show that the approximate volumetric deformation has the following form

$$\varepsilon_{ii}^h(\mathbf{x},t) = u_{i,i}^h = \varepsilon_{xx}^h + \varepsilon_{yy}^h = \sum_{I=1}^{NP} \mathbf{B}_I^{pT}(\mathbf{x}) \mathbf{d}_I(t) \tag{29}$$

Substituting Eqs. (24)-(27) into the weak form of Eq. (16) yields the following discrete equations

$$\begin{cases} \mathbf{K}\mathbf{d} - \mathbf{G}\mathbf{p} = \mathbf{f}^s \\ \mathbf{G}^T\dot{\mathbf{d}} + \mathbf{V}\dot{\mathbf{p}} + \mathbf{W}\mathbf{p} = \mathbf{f}^f \end{cases} \tag{30}$$

where

$$\mathbf{K} = \underset{I,J=1}{\overset{NP}{A}}[\mathbf{K}_{IJ}],\ \mathbf{G} = \underset{I,J=1}{\overset{NP}{A}}[\mathbf{G}_{IJ}],\ \mathbf{V} = \underset{I,J=1}{\overset{NP}{A}}[V_{IJ}],\ \mathbf{W} = \underset{I,J=1}{\overset{NP}{A}}[W_{IJ}] \tag{31}$$

$$\mathbf{d} = \underset{I=1}{\overset{NP}{A}}[\mathbf{d}_I],\ \mathbf{p} = \underset{I=1}{\overset{NP}{A}}[p_I],\ \mathbf{f}^s = \underset{I=1}{\overset{NP}{A}}[\mathbf{f}_I^s],\ \mathbf{f}^f = \underset{I=1}{\overset{NP}{A}}[f_I^f] \tag{32}$$

with A being the standard assembly operator (Hughes 2000). The corresponding sub-matricesand sub-vectors in Eqs. (31)-(32) are given by

$$\begin{cases} \mathbf{K}_{IJ} = \int_\Omega \mathbf{B}_I^{uT} \mathbf{C} \mathbf{B}_J^u d\Omega,\ \mathbf{G}_{IJ} = \int_\Omega \mathbf{B}_I^p \alpha \Psi_J d\Omega \\ V_{IJ} = \int_\Omega \Psi_I K_C^{-1} \Psi_J d\Omega,\ W_{IJ} = \int_\Omega \mathbf{B}_I^{pT} \kappa \mathbf{B}_J^p d\Omega \end{cases} \tag{33}$$

$$\begin{cases} \mathbf{f}_I^s = \int_\Omega \Psi_I \rho \mathbf{b} d\Omega + \int_{\Gamma^t} \Psi_I \bar{\mathbf{t}} d\Gamma \\ f_I^f = \int_\Omega \mathbf{B}_I^{pT} \kappa \rho_f \mathbf{g} d\Omega + \int_{\Gamma^q} \Psi_I \bar{q} d\Gamma \end{cases} \tag{34}$$

$\mathbf{C}$ is the plane-strain elasticity matrix

$$\mathbf{C} = \frac{E}{(1+v)(1-2v)} \begin{bmatrix} 1-v & v & 0 \\ v & 1-v & 0 \\ 0 & 0 & (1-v)/2 \end{bmatrix} \tag{35}$$

in which E and v are the Young's modulus and Poisson's ratio of the solid skeleton, respectively.

3.3 Strain smoothing nodal integration formulation

In the stabilized conforming nodal integration formulation (Chen *et al*. 2001), to achieve the spatial stability smoothed strain measure has been taken to nodally discretize the Galerkin weak form. Here for the coupled consolidation problem, the smoothing operation is invoked simultaneously on the strain $\boldsymbol{\varepsilon}^h$ and the pore pressure gradient ∇p in order to establish an efficient and stable meshfree algorithm

$$\tilde{\boldsymbol{\varepsilon}}^h(\mathbf{x}_L, t) = \frac{1}{area(\Omega_L)} \int_{\Omega_L} \boldsymbol{\varepsilon}^h(\mathbf{x}, t) d\Omega = \sum_{I=1}^{NP} \tilde{\mathbf{B}}_I^u(\mathbf{x}_L) \mathbf{d}_I(t) \tag{36}$$

$$\tilde{\nabla} p^h(\mathbf{x}_L, t) = \frac{1}{area(\Omega_L)} \int_{\Omega_L} \nabla p^h(\mathbf{x}, t) d\Omega = \sum_{I=1}^{NP} \tilde{\mathbf{B}}_I^p(\mathbf{x}_L) p_I(t) \tag{37}$$

where as shown in Fig. 1, Ω_L is the nodal representative domain of node $\mathbf{x}_L$ and it serves as a smoothing domain herein. $\tilde{\mathbf{B}}_I^u$ and $\tilde{\mathbf{B}}_I^p$ are the smoothed gradient matrices. By substituting Eqs.

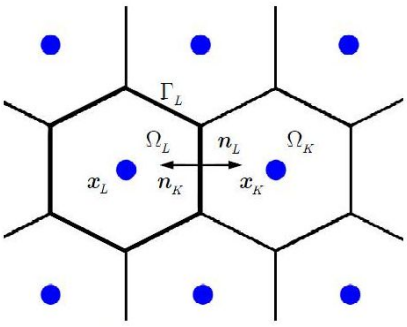

Fig. 1 Schematic illustration of nodal representative domain

(26) and (8 into Eqs. (36) and (37) and further invoking the divergence theorem, it is straightforward to show $\tilde{\mathbf{B}}_I^u$ and $\tilde{\mathbf{B}}_I^p$ take the following form

$$\tilde{\mathbf{B}}_I^u(\mathbf{x}_L)=\begin{bmatrix}\tilde{\Psi}_{I,x}(\mathbf{x}_L) & 0\\ 0 & \tilde{\Psi}_{I,y}(\mathbf{x}_L)\\ \tilde{\Psi}_{I,y}(\mathbf{x}_L) & \tilde{\Psi}_{I,x}(\mathbf{x}_L)\end{bmatrix} \tag{38}$$

$$\tilde{\mathbf{B}}_I^p(\mathbf{x}_L)=\begin{bmatrix}\tilde{\Psi}_{I,x}(\mathbf{x}_L)\\ \tilde{\Psi}_{I,y}(\mathbf{x}_L)\end{bmatrix} \tag{39}$$

and the smoothed gradient of the meshfree shape function is given by

$$\tilde{\Psi}_{I,i}(\mathbf{x}_L)=\frac{1}{area(\Omega_L)}\int_{\Gamma_L}\Psi_I(\mathbf{x})n_i d\Gamma \tag{40}$$

with Γ_L being the boundary of Ω_L and n_i denoting the outward normal of Γ_L as shown in Fig. 1.

Moreover in this study to construct a consistent SCNI consolidation formulation, the following smoothing operation is introduced for the meshfree shape function Ψ_I that is involved in the evaluation of the matrices of *V* and *W*

$$\tilde{\Psi}_I(\mathbf{x}_L)=\frac{1}{length(\Gamma_L)}\int_{\Gamma_L}\Psi_I(\mathbf{x})d\Gamma \tag{41}$$

Employing the smoothed measures defined in Eqs. (36)-(41), a nodal integration of the stiffness and force terms in Eqs. (33) and (34) gives

$$\begin{cases}\mathbf{K}_{IJ}=\sum_{L=1}^{NP}\tilde{\mathbf{B}}_I^{uT}(\mathbf{x}_L)\mathbf{C}\tilde{\mathbf{B}}_J^u(\mathbf{x}_L)area(\Omega_L)\\ \mathbf{G}_{IJ}=\sum_{L=1}^{NP}\tilde{\mathbf{B}}_I^p(\mathbf{x}_L)\mathbf{C}\tilde{\Psi}_J(\mathbf{x}_L)area(\Omega_L)\\ V_{IJ}=\sum_{L=1}^{NP}\tilde{\Psi}_I(\mathbf{x}_L)K_C^{-1}\tilde{\Psi}_J\mathbf{x}_L area(\Omega_L)\\ W_{IJ}=\sum_{L=1}^{NP}\tilde{\mathbf{B}}_I^{pT}(\mathbf{x}_L)\kappa\tilde{\mathbf{B}}_J^p(\mathbf{x}_L)area(\Omega_L)\end{cases} \tag{42}$$

$$\begin{cases} \mathbf{f}_I^s = \sum_{L=1}^{NP} \tilde{\Psi}_I(\mathbf{x}_L)\rho \mathbf{b} area(\Omega_L) + \sum_{B=1}^{NB} \tilde{\Psi}_I(\mathbf{x}_B)\bar{\mathbf{t}}(\mathbf{x}_B) l_B \\ f_I^f = \sum_{L=1}^{NP} \tilde{\mathbf{B}}_I^{pT}(\mathbf{x}_L)\kappa\rho_f \mathbf{g} area(\Omega_L) + \sum_{B=1}^{NB} \tilde{\Psi}_I(\mathbf{x}_B)\bar{q}(\mathbf{x}_B) l_B \end{cases} \tag{43}$$

where *NB* denotes the number of nodes associated with the natural boundary and l_B is the corresponding integration weight.

Finally the system of equations of (30) can be advanced in a time interval $[t_n,\ t_{n+1}]$ by the generalized trapezoidal rule (Hughes 2000)

$$\begin{cases} \mathbf{d}_{n+1} = \mathbf{d}_n + \Delta t \dot{\mathbf{d}}_{n+\theta}, \quad \dot{\mathbf{d}}_{n+\theta} = (1-\theta)\dot{\mathbf{d}}_n + \theta \dot{\mathbf{d}}_{n+1} \\ \mathbf{p}_{n+1} = \mathbf{p}_n + \Delta t \dot{\mathbf{p}}_{n+\theta}, \quad \dot{\mathbf{p}}_{n+\theta} = (1-\theta)\dot{\mathbf{p}}_n + \theta \dot{\mathbf{p}}_{n+1} \end{cases} \tag{44}$$

where $\theta \in [0,\ 1]$, $\Delta t = t_{n+1} - t_n$. By enforcing Eq. (30) at $t = t_{n+1}$ and using Eq. (44), we have the following time-stepping equation

$$\begin{bmatrix} \theta\Delta t\mathbf{K} & -\theta\Delta t\mathbf{G} \\ \mathbf{G}^T & \mathbf{V} + \theta\Delta t\mathbf{W} \end{bmatrix} \begin{Bmatrix} \dot{\mathbf{d}} \\ \dot{\mathbf{p}} \end{Bmatrix}_{n+1} = \begin{Bmatrix} \mathbf{f}^s \\ \mathbf{f}^f \end{Bmatrix}_{n+1} - \begin{bmatrix} \mathbf{K} & \mathbf{G} \\ \mathbf{0} & \mathbf{W} \end{bmatrix} \left(\begin{Bmatrix} \mathbf{d} \\ \mathbf{p} \end{Bmatrix}_n + (1-\theta)\Delta t \begin{Bmatrix} \dot{\mathbf{d}} \\ \dot{\mathbf{p}} \end{Bmatrix}_n \right) \tag{45}$$

4. Numerical examples

4.1 Column squeezing problem

As shown in Fig. 2, a porous column is surrounded by rigid and impermeable walls. The geometry and material properties are: height $H = 1m$ and width $L = 0.2m$, Young's modulus $E = 3\times10^4 Pa$, Poisson's ratio $v = 0.2$, intrinsic permeability $\hat{\kappa} = 10^{-9} m^2$ and fluid viscosity $\mu_f = 10^{-2} Pa\cdot \mathrm{s}$. Meanwhile, the column top is subjected to a pressure $\sigma_0 = -p_0 = -10^3 Pa$ and it's under free-drain condition. When the solid and fluid phases assumed intrinsically incompressible and the gravity is neglected, the analytical solution for this problem is (Murad and Loula 1992)

$$\begin{cases} u_D = 1 - x_D - \sum_{k=0}^{\infty} \frac{2}{\eta^2} \cos(\eta x_D) \exp(-\eta^2 t_D) \\ p_D = \sum_{k=0}^{\infty} \frac{2}{\eta} \sin(\eta x_D) \exp(-\eta^2 t_D) \end{cases}, \ \eta = \frac{(2k+1)\pi}{2} \tag{46}$$

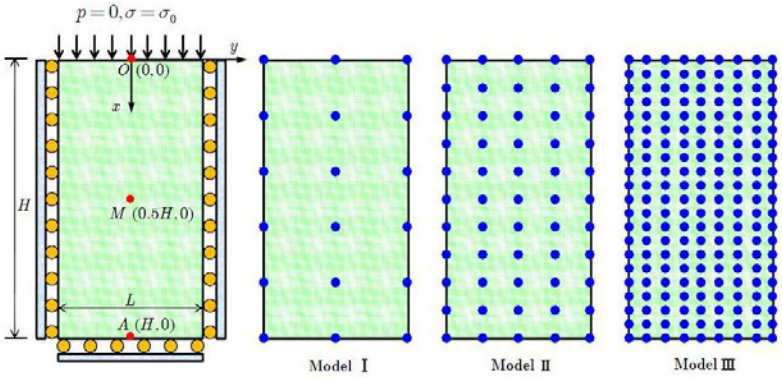

Fig. 2 Description and meshfreediscretizatons of the column squeezing problem

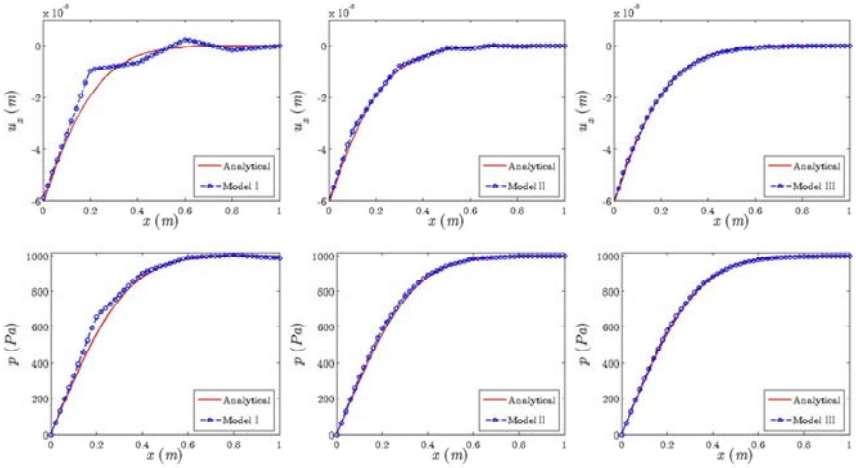

Fig. 3 The displacement and pore pressure distribution along line *OA* of the column squeezing problem at $t = 10s$

where

$$\begin{cases} x_D = x/H,\ t_D = \dfrac{E(1-v)\hat{\kappa}t}{(1+v)(1-2v)\mu H^2} \\ u_D = u\dfrac{E(1-v)}{(1+v)(1-2v)\sigma_0 H^2},\ p_D = p/p_0 \end{cases} \tag{47}$$

To examine the convergence of the present formulation, as shown in Fig. 2 three meshfree discretziations of 18 nodes, 55 nodes, and 189 nodes are used for numerical simulation. A linear basis function and the cubic B-spline kernel function with a normalized support size of 1.5 are adopted for the meshfree shape function. As for the time integration, the implicit backward-Euler method with $\theta = 1$ is utilized with $\Delta t = 1s$ and the time history for the simulation is $T = 1000s$. The results of both the displacement and the pore pressure along the line *OA* with

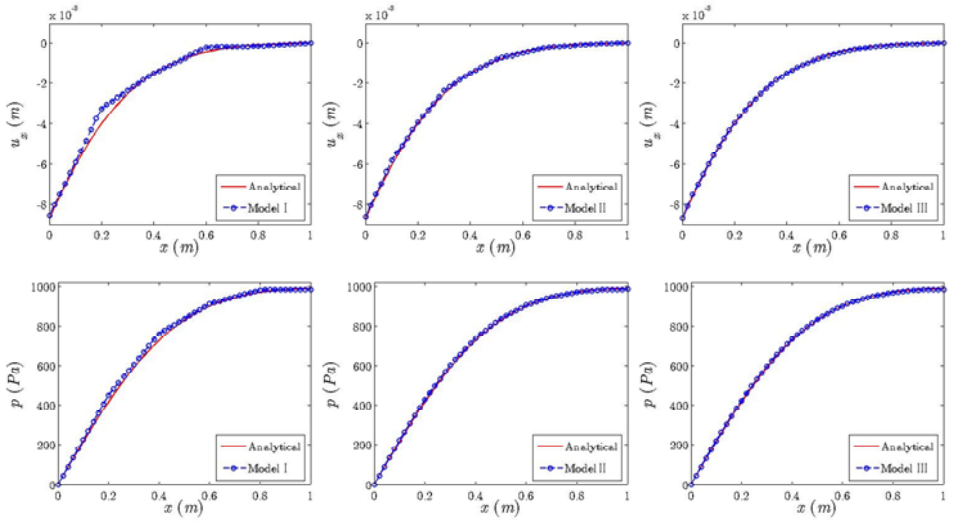

Fig. 4 The displacement and pore pressure distribution along line *OA* of the column squeezing problem at $t = 20s$

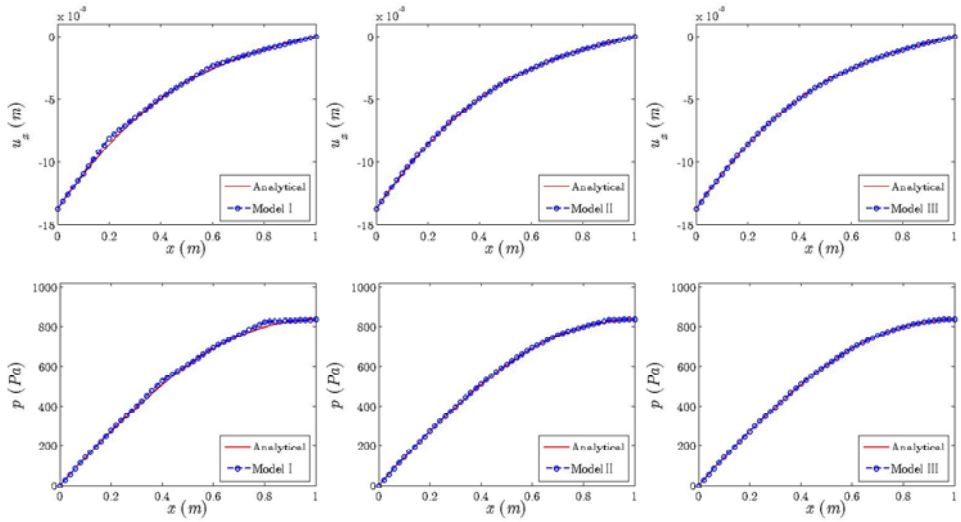

Fig. 5 The displacement and pore pressure distribution along line *OA* of the column squeezing problem at $t = 50s$

various discretziations are reported in Figs. 3-5 for different time steps. Comparison with the analytical solutions shows the present formulation gives very good convergence performance.

Meanwhile, the time history of the displacement and pore pressure at the sampling points *O*, *M*and *A* are illustrated in detail in Fig. 6 and once again the solutions approach quickly to their analytical counterparts.

4.2 Cubic sponge squeezing problem

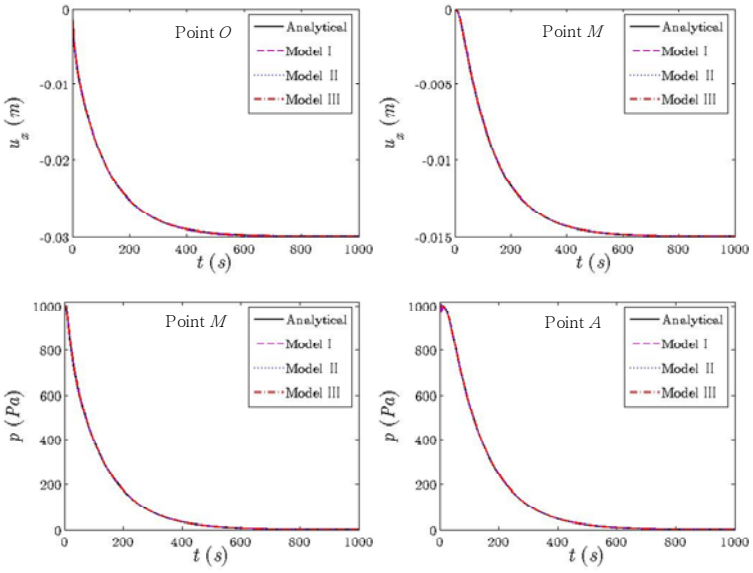

Fig. 6 Comparison of the displacement distributions over the problem domain at t = 20s, 50s for the spongesqueezing problem

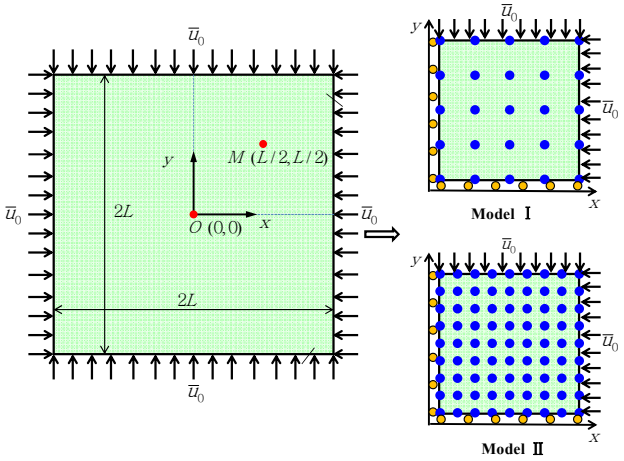

Fig. 7 Comparison of the displacement distributions over the problem domain at t = 20s, 50s for the spongesqueezing problem

Simulation of the cubic sponge squeezing process is a benchmark test for the consolidation algorithm. This problem can be modeled by a square sponge with length of 2L as shown in Fig. 7. All four boundaries are under impermeable condition and the sponge is squeezed instantaneously on the four sides by an applied inward displacement $\bar{u}_0$. It is assumed that the solid and fluid phases are intrinsically incompressible and the gravity effect is neglected as well. The geometry, material and loading properties of this problem are: L = 2m, Young's modulus E = $6\times10^7 Pa$, Poisson's ratio ν = 0.3, permeability $\kappa = 3\times10^{-10} m^2/(Pa\cdot s)$, applied displacement $\bar{u}_0 = 0.1m$.

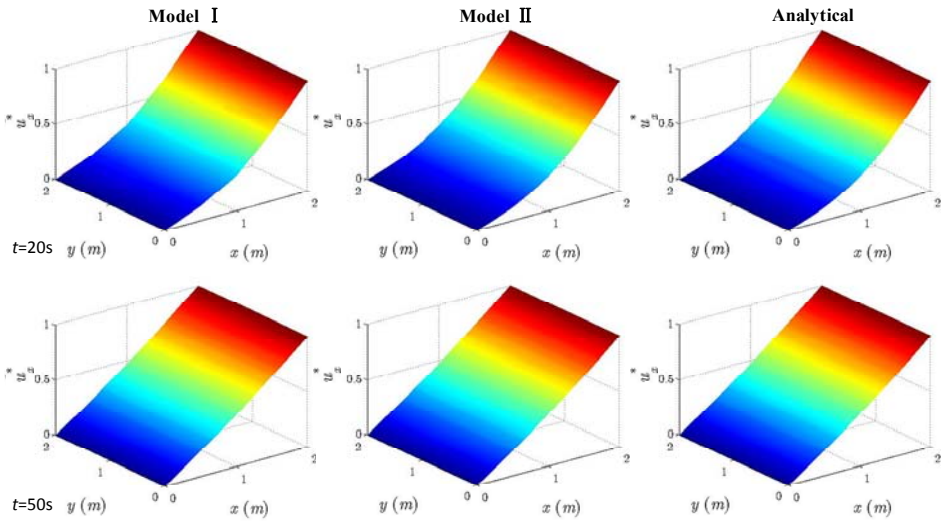

Fig. 8 Comparison of the displacement distributions over the problem domain at t = 20s, 50s for the sponge squeezing problem

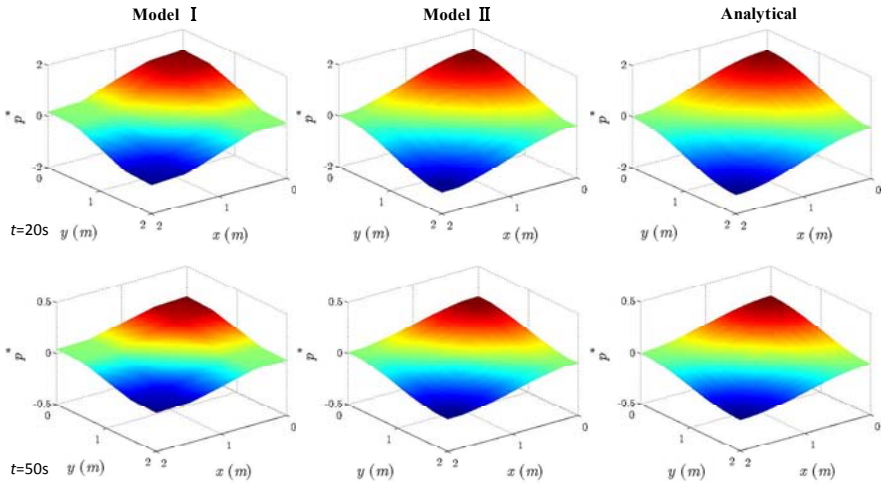

Fig. 9 Comparison of the pore pressure distributions over the problem domain at t = 20s, 50s for the sponge squeezing problem

The analytical solution for this problem is given by Kaasschieter and Frijns (2003)

$$\begin{cases} u_i(\mathbf{x},t) = \dfrac{\overline{u}_0}{L}x_i + L\sum\limits_{k=1}^{\infty}\dfrac{2\overline{u}_0}{k\pi L}(-1)^k \times \sin(\dfrac{k\pi x_i}{L})\exp(-\dfrac{k^2\pi^2 t}{D}) \\ p(\mathbf{x},t) = \dfrac{E(1-v)}{(1+v)(1-2v)}\sum\limits_{k=1}^{\infty}\dfrac{2\overline{u}_0}{L}(-1)^k \times \sum\limits_{i=1}^{2}\cos(\dfrac{k\pi x_i}{L})\exp(-\dfrac{k^2\pi^2 t}{D}) \end{cases} \tag{48}$$

with the parameter D being

$$D=\frac{L^2(1+v)(1-2v)}{E(1-v)\kappa} \tag{49}$$

Due to the two-fold symmetry, only one quarter sponger is used for the meshfree modeling with proper symmetry conditions. Two meshfreed is cretziations with 25 nodes and 81 nodes are employed in the present computation as shown in Fig. 7. The meshfree shape functions are formulated using the linear basis function and the cubic B-spline kernel function with a normalized support size of 1.5. The backward Euler scheme is used for the time integration, and the time step and total simulation time are $\Delta t=1s$ and $T=170s$, respectively. The displacement and pore pressure distributions over the problem domain at $t=20s,\ 50s$ are compared with the analytical solutions in Figs. 8-9, where for convenience of comparison the normalized displacement $u_i^*=u_i/u_0$ and the normalized pressure $p^*=-pL(1+v)(1-2v)/[E(1-v)u_0]$ are used. Moreover, the time history of the displacement and pore pressure at the point *M* as indicated in Fig. 7 is plotted in Fig. 10. The numerical results show excellent agreement between the meshfree and analytical solutions.

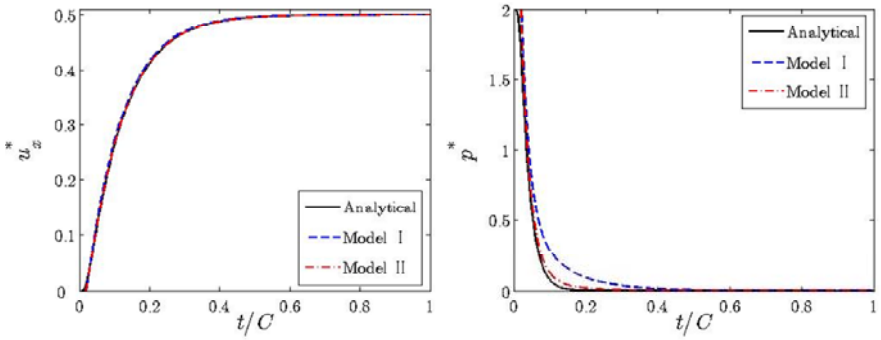

Fig. 10 Time history of the displacement and pore pressure at the point *M* for the spongesqueezing problem

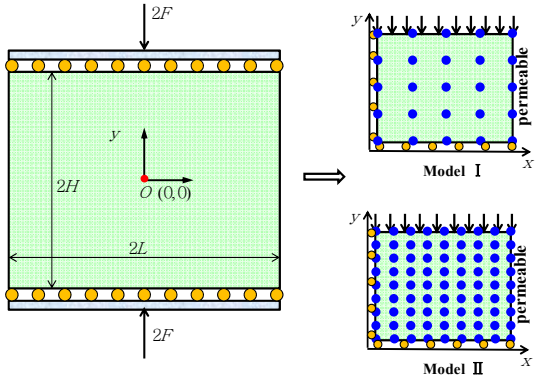

Fig. 11 Mandel's problem and its meshfeediscretizations

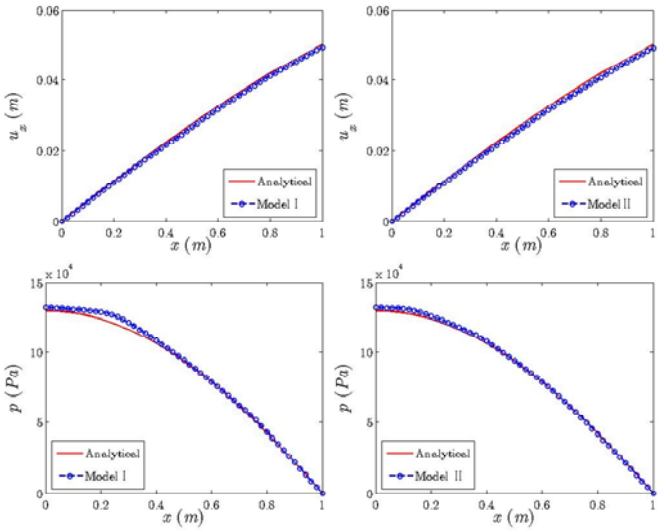

Fig. 12 Comparison of the displacement and pore pressure at t = 300s with different meshfreediscretizations for the Mandel's problem

4.3 Mandel's consolidation problem

The Mandel's consolidation problem as shown in Fig. 11 refers to a porous rectangle specimen with width $2L$ and height $2H$ which is bounded by two rigid and impermeable plates at the top and bottom, respectively. This problem is a typical two dimensional consolidation process since the third direction is assumed infinitely long. The consolidation process is activated by a pair load of $2F$ (per unit length of thickness direction) on the upper and lower plates simultaneously. For this problem, the geometry, material and loading parameters are: $L = H = 1m$, Young's modulus $E = 6\times10^6\,Pa$, Poisson's ratio $v = 0.2$, permeability $\kappa = 5\times10^{-10}\,m^2/(Pa\cdot\mathrm{s})$, applied loading $F = 1MPa$. In case that intrinsic incompressibility is assumed for the porous media, by neglecting the gravity the analytical solutioncan be found as (Cheng and Detournay 1988)

$$\begin{cases} u_x(\mathbf{x},t) = \left[\dfrac{Fv}{2\mu L} - \dfrac{Fv_u}{\mu L}\displaystyle\sum_{i=1}^{\infty}\frac{\sin\alpha_i\cos\alpha_i}{\alpha_i-\sin\alpha_i\cos\alpha_i}\exp(-\alpha_i^2 ct/L^2)\right]x \\ \quad + \dfrac{F}{\mu}\displaystyle\sum_{i=1}^{\infty}\frac{\cos\alpha_i}{\alpha_i-\sin\alpha_i\cos\alpha_i}\sin\frac{\alpha_i x}{L}\exp(-\alpha_i^2 ct/L^2) \\ p(\mathbf{x},t) = \dfrac{2FS(1+v_u)}{3\mu L}\displaystyle\sum_{i=1}^{\infty}\frac{\sin\alpha_i}{\alpha_i-\sin\alpha_i\cos\alpha_i}(\cos\frac{\alpha_i x}{L}-\cos\alpha_i)\exp(-\alpha_i^2 ct/L^2) \end{cases} \tag{50}$$

where S is the Skempton's pore pressure coefficient, v_u is the undrained Poisson's ratio, c is the consolidation coefficient

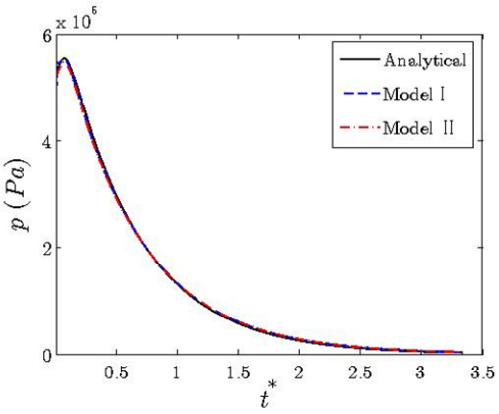

Fig. 13 Time history of the pore pressure at the point O for the Mandel's problem

$$c = \frac{2\kappa S^2 G(1-v)(1+v_u)^2}{9(1-v_u)(v_u-v)}, \quad \tan\alpha_i = \alpha_i \frac{1-v}{v_u-v} \tag{51}$$

In this problem, the Skempton's pore pressure coefficient and undrained Poisson's ratio are $S=1$ and $v_u=0.5$.

The meshfree discretizations with 25 and 81 nodes for the Mandel's problem are also shown in Fig. 11. The linear basis function and a 1.5 normalized support size are adopted to build the meshfree approximation. The backward Euler method with a time step of $\Delta t = 1s$ is invoked to update the discrete equations. The total simulation time is $T = 1000s$. The results of displacement and pore pressure are compared with the analytical solutions at the time $t = 300s$ in Fig. 12. Moreover the time history of the pore pressure at the point O is compared with the analytical solutions in Fig. 13 where the normalized time $t^* = ct/L^2$ is used. The numerical results demonstrate very favorable solution accuracy can be obtained by the present meshfree method with relatively coarse discretizations.

5. Conclusions

A stabilized conforming nodal integration Gakerlin meshfree method was presented for numerical simulation of consolidation process in saturated porous media. This method is based upon consistent strain smoothing operation on the strain field as well as the pore pressure gradient field, which yield smoothed nodal strain and pore pressure gradient measures defined in a nodal representative domain. At the same time a smoothed nodal shape function was also introduced as an average of the boundary integral of the meshfree shape function in the nodal representative domain. Thereafter the smoothed nodal strain, pore pressure gradient and shape function were invoked simultaneously to establish the nodally integrated discrete equations governing the consolidation process. As the final step, the generalized trapezoidal rule was adopted for temporal discretization and equation updating. Three benchmark sampling problems, the column squeezing

problem, the sponge squeezing problem and the Mandel's consolidation problem were analyzed by the present method. The numerical results compare very well with the analytical solutions which show that the proposed formulation provides a very effective way for analysis of consolidation problems.

Acknowledgements

The financial support of this work by the National Natural Science Foundation of China (11222221) is gratefully acknowledged.

References

Atluri, S.N. and Shen, S.P. (2002), *The Meshless Local Petrov-GalerkinMethod*, Tech Science Press.

Babuška, I., Banerjee, U. and Osborn, J.E. (2003), "Survey of meshless and generalized finite element methods: a unified approach", *ActaNumer.*, **12**(1), 1-125.

Beissl, S. and Belytschko, T. (1996), "Nodal integration of the element-free Galerkin method", *Comput.Meth.Appl. Mech. Eng.*, **139**(1-4), 49-64.

Belytschko, T., Lu, Y.Y. and Gu, L. (1994), "Element-free gakerkin methods", *Int. J. Num. Meth. Eng.*, **37**(2), 229-256.

Biot, M.A. (1941), "General theory of three-dimensional consolidation", *J.Appl. Phys.*, **12**(2), 155-169.

Biot, M.A. (1956), "Theory of propagation of elastic waves in a fluid-saturated porous solid, I: Low-frequency-range", *J. Acout. Soc. Ame.*, **28**(2), 168-178.

Chen, J.S., Chi, S.W. and Hu, H.Y. (2011), "Recent developments in stabilized Galerkin and collocation meshfree methods", *Comput. Assist. Mech. Eng. Sci.*, **18**, 3-21.

Chen, J.S., Pan, C., Wu, C.T. and Liu, W.K. (1996), "Reproducing kernel particle methods for large deformation analysis of nonlinear structures", *Comput. Meth. Appl. Mech. Eng.*, **139**(1-4), 195-227.

Chen, J.S. and Wang, D. (2006), "A constrained reproducing kernel particle formulation for shear deformable shell in cartesian coordinates", *Int. J. Num. Meth. Eng.*, **68**(2), 151-172.

Chen, J.S., Wu, C.T. and Belytschko, T. (2000), "Regularization of material instabilities by meshfree approximations with intrinsic length scales", *Int. J. Num. Meth. Eng.*, **47**(7), 1301-1322.

Chen, J.S., Wu, C.T., Yoon, S. and You, Y. (2001), "A stabilized conforming nodal integration for Galerkinmeshfree methods", *Int. J. Num. Meth. Eng.*, **50**(2), 435-466.

Chen, J.S., Yoon, S. and Wu, C.T. (2002), "Nonlinear version of stabilized conforming nodal integration for Galerkinmeshfree methods", *Int. J. Num. Meth. Eng.*, **53**(12), 2587-2615.

Cheng, A.H.D. and Detournay, E. (1988), "A direct boundary element method for plane strain poro-elasticity", *Int. J. Num. Anal.Meth.Geom.*, **12**(5), 551-72.

Cui, L., Cheng, A.H.D. and Kaliakin, V.N. (1996), "Finite element analyses of anisotropic poroelasticity: a generalized mandel's problem and an inclined borehole problem", *Int. J. Numer. Anal. Meth. Geom.*, **20**(6), 381-401.

Guan, P.C., Chi, S.W., Chen, J.S., Slawson, T.R. and Roth, M.J (2011), "Semi-lagrangian reproducing kernel particle method for fragment-impact problems", *Int. J. Impact Eng.*, **38**(12), 1033-1047.

Hughes, T.J.R. (2000), *The finite element method: linear static and dynamic finite element analysis*, Dover publications,Mineola, NY.

Kaasschieter, E.F. and Frijns, A.J.H. (2003), "Squeezing a sponge: a three-dimensional a nalytical solution in poroelasticity", *Comput. Geosci.*,7(1), 49-59.

Korsawe, J., Starke, G., Wang, W. and Kolditz, O. (2006), "Finite element analysis of poro-elastic consolidation in porous media: Mixed and standard approaches", *Math.*, **195**(9-12), 1096-1115.

Lancaster, P. and Salkauskas, K. (1981), "Surfaces generated by moving least squares methods", *Math.Comput.*,**37**(155), 141-158.

Li, S. and Liu, W.K. (2004), *MeshfreeParticle Methods*, Springer-Verlag.

Liu, G.R. (2009), *Mesh Free Methods: Moving Beyond the Finite Element Mehod,*2ndEdition, CRC Press.

Liu, W.K., Jun, S. and Zhang, Y.F. (1995), "Reproducing kernel particle methods", *Int. J.Numer.Fluids*, **20**(8-9), 1081-1106.

Murad, M. and Loula, A. (1992), "Improved accuracy in finite element analysis of Biot's consolidation problem", *Comput.Meth. Appl. Mech. Eng.*, **95**(3), 359-382.

Samimi, S. and Pak, A. (2012), "Three-dimensional simulation of fully coupled hydro-mechanical behavior of saturated porous media using Element Free Galerkin (EFG) method", *Comput.Geotech.*,**46**, 75-83.

Schönewald, A., Soares, D. and von Estorff, O. (2012), "A smoothed radial point interpolation method for application in porodynamics", *Computat. Mech.*, **50**(4), 433–443

Wang, D. and Chen, J.S. (2004), "Locking-free stabilized conforming nodal integration for meshfreemindlin-reissner plate formulation", *Comput. Meth. Appl. Mech. Eng.*, **193**(12-14), 1065-1083.

Wang, D. and Chen, J.S. (2008), "A Hermite reproducing kernel approximation for thin plate analysis with sub-domain stabilized conforming integration", *Int. J. Numer. Meth. Eng.*, **74**(3), 368-390.

Wang, D., Li, Z., Li, L. and Wu, Y. (2011), "Three dimensional efficient meshfree simulation of large deformation failure evolution in soil medium", *Sci. China-Technol. Sci.*,**54**(3), 573-580.

Wang, D. and Lin, Z. (2011), "Dispersion and transient analyses of hermite reproducing kernel galerkinmeshfree method with sub-domain stabilized conforming integration for thin beam and plate structures", *Comput. Mech.*, **48**(1), 47-63.

Zienkiewicz, O.C. and Shiomi, T. (1984), "Dynamic behaviour of saturated porous media; the generalized Biot formulation and its numerical solution", *Int. J. Numer. Anal. Meth. Geom.*, **8**(1), 71-96.